Damping mechanisms in a tip-mass piezoelectric cantilever system

Abinayaa Dhanaghopal[1], Lawrence D. Little[1], Yahriel Salinas-Reyes[1], Martin Thuo[2] and Thomas Ward[1]
[1]*Department of Aerospace Engineering, Iowa State University, Ames, IA 50011-2271 and*
[2]*Department of Material Science and Engineering, Iowa State University, Ames, IA 50011-0000*
(Dated:)

Here we characterize the damping response from a commercial piezoelectric transducer when it is subjected to free-vibrations. The problem under study is an electromechanical problem and hence a combination of dimensionless parameters including the natural frequency of the system, are used to study and understand the damping characteristics of the tip-mass-piezoelectric system. Rectangular prisms with varying aspect ratios(0.5-3.0) are loaded onto two flexible piezoelectric transducers rendering the setup to resemble a cantilever tip-mass system.To directly visualize the effect of tip displacement on the voltage generated, high-speed imaging studies of the cantilever are performed in addition to separate measurements of the voltage response using an oscilloscope. In this paper, we will discuss how these results can further studies into the development of efficient energy harvesters.

PACS numbers:

In this manuscript we present experimental and computational data for the free vibrations of a tip-mass piezoelectric cantilever system. Here we are interested in developing robust dynamic models that may be used as a test bed for understanding control of dynamic behavior that arises in these types of complex systems [1–7]. The Euler-Bernoulli equations with coupled linear piezoelectric deformation equations govern the cantilever's displacement in the small amplitude vibration limit. These equations were developed in other publications for the purpose of single mode vibration analysis [1]. Here, we utilize those equations through a slight modification to study the small amplitude vibration of a damped cantilever with a mass at the tip undergoing free-vibration. The system yields fully-transient dynamics, and understanding the role that damping can play in generating power from these piezo-electric systems is of interests. It has been shown that adding a mass (vibration inducing body) at the tip of piezoelectric cantilevers results in a tremendous increase in the efficiency of energy harvesters [8].

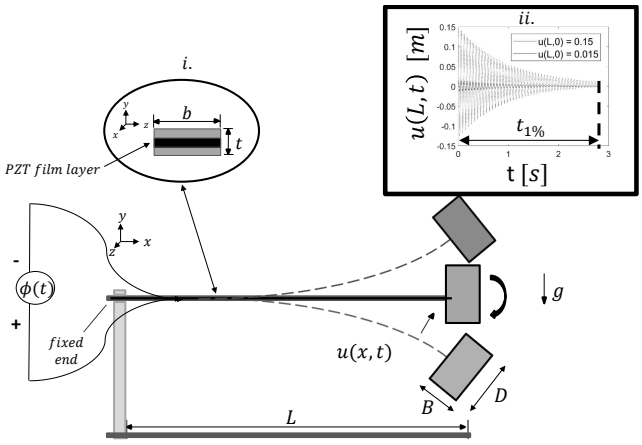

FIG. 1: Problem schematic. *i* PZT layer cross section. *ii* Plot of displacement versus time for 2 initial displacements of a damped Euler-Bernoulli cantilever with $\pi_4 = 4$. Both attenuate to 1% of that initial displacement at the same elapsed time.

Consider a flexible cantilever made of laminated polymer piezo-electric material such that the piezo-electric material lies along the cantilever's neutral axis. We seek to study unsteady motion of this cantilever along its transverse axis assuming displacements with the generic form $u(x,t)$. The other variables are cantilever composite density, ρ, composite cross sectional area, $A = t_c L$, composite elastic modulus, E, and composite area moment of inertia, I. We include net external (linear viscous, μ_1), and internal (Kelvin-Voigt, μ_2) damping [9] for a homogeneous cantilever. The relevant electrical properties are the piezoelectric film capacitance C_f, the film resistance R_f, and the electro-mechanical coupling term $\alpha = d_{31} E_p h_{pc} b$ where d_{31} is the strain per electric field coincident with the direction of axial strain (1) and polarization (3); E_p is the piezoelectric elastic modulus; h_{pc} is the distance of piezoelectric center to the neutral axis and b is the beam width. Attached to the cantilever's tip is a mass m_T with cross-section long dimension B and height D. The cantilever with tip-mass natural frequency is denoted ω_N, and natural frequency (first mode vibration) in the absence of the tip-mass $m_T = 0$ is denoted ω_{N_0}. Figure 1 shows a schematic of the problem proposed in this study where the neutral axis is positioned with its length along the x-axis.

In Ref. [1] the authors develop equations of motion for a piezoelectric material placed along the neutral axis of a cantilever for the problem of base excitation (forced vibration). The equation set consisted of coupled Euler-Bernoulli beam equation and an integrated electric displacement equation that results in a two component current conservation equation. Coupling was achieved by considering the composite cantilever's total internal moment as the sum of a bending stiffness moment, and a moment generated from the product of an induced voltage potential, ϕ, and the E-M coupling term α. An unsteady

voltage was considered uniform over the length spanning the piezoelectric material, therefore the coupling appears through boundary conditions (although the authors in Ref. [1] use Heaviside functions to include the E-M coupling moment in the main equation in order to perform a modal analysis through separation of variables).

Here, the same equations of motion are made dimensionless by scaling lengths with the non-deformed cantilever length L and time with the frequency $\omega = \sqrt{EI/\rho AL^4}$ (note that ω_{N_0} is proportional to ω [10, 11]). The resulting dimensionless independent and dependent variables are $u^* = u/L$, $x^* = x/L$, $v^* = v/(\omega L)$, $\phi^* = \phi C_f/\alpha$ and $t^* = \omega t$; and the dimensionless form of the coupled Euler-Bernoulli and electric current conservation equations are

$$\frac{\partial u^*}{\partial t^*} = v^* \tag{1}$$

$$\frac{\partial v^*}{\partial t^*} = -\pi_1 v^* - \pi_2 \frac{\partial^4 v^*}{\partial x^{4*}} - \frac{\partial^4 u^*}{\partial x^{4*}} \tag{2}$$

$$\frac{\partial \phi^*}{\partial t^*} = \pi_3 \phi^* - \int_0^1 \frac{\partial^2 v^*}{\partial x^{2*}} dx. \tag{3}$$

Solutions for the linear PDE can be found by using the boundary conditions for a cantilever with E-M coupling and a tip-mass [9], where at $x^* = 0$ we apply a fixed and symmetry condition:

$$u^*(0, t^*) = 0 \tag{4a}$$

$$\frac{\partial u^*}{\partial x^*} = 0 \tag{4b}$$

and at $x^* = 1$ we apply conservation of moments and force, respectively,

$$\frac{\partial^2 u^*}{\partial x^{2*}} + \pi_2 \frac{\partial^2 v^*}{\partial x^{2*}} = \pi_4 \frac{\partial^2 v^*}{\partial t^* \partial x^*} - \pi_5 \phi^* \tag{5a}$$

$$\frac{\partial^3 u^*}{\partial x^{3*}} + \pi_2 \frac{\partial^3 v^*}{\partial x^{3*}} = \pi_4 \frac{\partial v^*}{\partial t^*}. \tag{5b}$$

Notice we include the rotatory inertia term in the tip-moment conservation equation. The dimensionless variables are defined

$$\pi_1 = \frac{\mu_1}{\rho A \omega}, \quad \pi_2 = \frac{\mu_2 \omega}{E}, \quad \pi_3 = \frac{1}{C_f R_f \omega}, \tag{6}$$

$$\pi_4 = \frac{m_T}{m}, \quad \text{and} \quad \pi_5 = \frac{\alpha^2 L}{C_f EI}. \tag{7}$$

The dimensionless parameters represent: dimensionless viscous μ_1 and Kelvin-Voigt μ_2 damping coefficients, dimensionless inverse piezoelectric film resistance R_f, dimensionless tip-mass m_T and a dimensionless E-M coupling α.

Spatial derivatives in (1)-(3) and first derivative boundary condition in (5) were discretized using 4^{th} order accurate finite differences [12]. The tip-momentum and force conservation boundary conditions required much higher order accuracy (7^{th} order accuracy) to ensure unique solutions for the 5^{th} order spatial derivatives that appear after substitution of Eq. (2) into (6). The integral in (3) was computed using a trapezoidal rule. The equations were advanced in time using an adaptive 4^{th} order accurate Runge-Kutta-Merson (RKM) time stepping algorithm [13]. There were $n = 50$ interior grid points. The precision was set to 1×10^{-8} for all of the data presented here. The algorithm was written and implemented using an in-house code written in Fortran programming language.

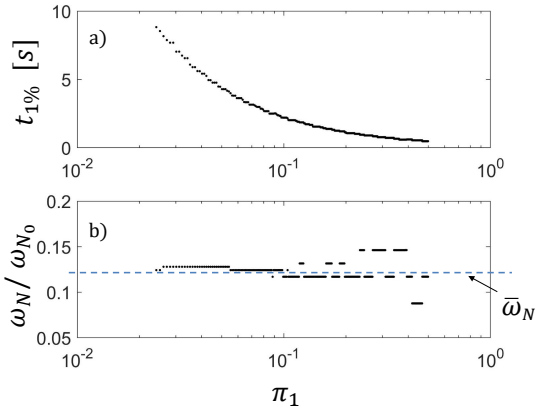

FIG. 2: Plot of a) $t_{1\%}$ and, b) natural frequency ω_N normalized by natural frequency for $\pi_4 = 0$ i.e. ω_{N_0}, with both plotted versus dimensionless viscous damping coefficient π_1 ($\pi_2 = 0$). A value of $\pi_4 = 4$ and $\omega \approx 120$ Hz was used for these calculations.

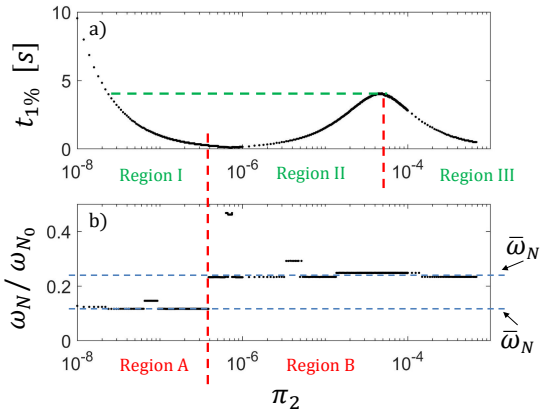

FIG. 3: Plot of a) $t_{1\%}$ and, b) natural frequency ω_N normalized by natural frequency for $\pi_4 = 0$ i.e. ω_{N_0}, with both plotted versus dimensionless viscous damping coefficient π_2 ($\pi_1 = 0$). A value of $\pi_4 = 4$ and $\omega \approx 120$ Hz was used for these calculations.

Solutions to the set of equations can be used to estimate the unknown damping coefficients μ_1 or μ_2 for a cantilever undergoing free-vibration [14]. We are assuming that the damping coefficient is independent of

any external forcing and does not vary with time. To estimate the coefficients we keep in mind that any displacement of the beam from its initial position should result in an underdamped system. In Fig. 1, with $\pi_4 = 4$ and $\pi_2 = 0.0001$ we show a solution to the governing equations for the problem of free-vibration that resulted in an underdamped system. Notice that for 2 different initial conditions, $u(L,0) = 0.15$ and 0.015 m, and with all other parameters being equal (including dimensionless frequency $\omega = 120$ Hz), that the two underdamped systems reach 1% of their initial displacement at the same time, denoted $t_{1\%}$. The value 1% is not unique, and any fraction below 40% appears to follow the same trend; though, there was noticeable difference in the normalized natural frequency that is measured as we computed the 1% times. Here, in Figs. 2(a)-3(a) we show the computed normalized $t_{1\%}$ for $0.02 < \pi_1 < 0.5$ with $\pi_2 = 0$ and $1 \times 10^{-8} < \pi_2 < 7 \times 10^{-4}$ with $\pi_1 = 0$, respectively. In Fig. 2(a) the data asymptotes to zero as the dimensionless damping coefficient is increased, but in Fig. 3(a) the initial $t_{1\%}$ values asymptote to zero then increase to a local maximum before another asymptote to zero, forming 3 regions I, II and III. This computational result suggests for systems where internal damping is present at least 3 values of π_2 can exist if $t_{1\%}$ is less than the value of the local maximum (horizontal dashed line). In

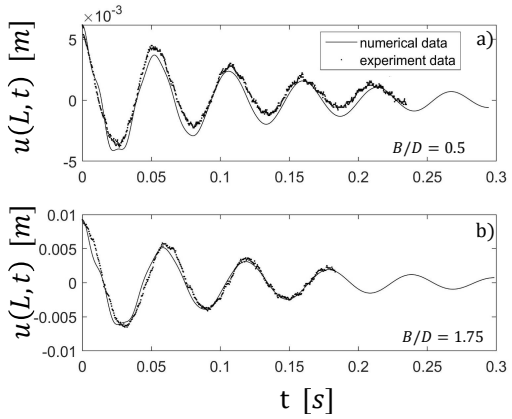

FIG. 4: Plots of free-vibration tip displacement of a PZT cantilever and tip-mass system. The experiment parameters were a) $B/D = 0.5$, $\pi_4 = 3.0$, and b) $B/D = 1.75$, $\pi_4 = 2.45$ with measured natural frequencies $\omega_N =$ a) 20.2 and b) 18.8 Hz. Also shown in each plot are results from computation using the same parameters with $\pi_1 = 0$, $\pi_2 =$ a) 8.33×10^{-8} and b) 1.1×10^{-7}.

Figs. 2(b)-3(b) we show the corresponding normalized natural frequencies for the same range of dimensionless damping coefficients as in 2(a)-3(a). In Fig. 2(b) there is a narrow range of values that span the data with the average $\bar{\omega}_N \approx 0.12$. In Fig. 3(b) there are 2 average values: the first is computed for π_2 values less than the first asymptotes minimum (Region A), and the second for the values greater than this first asymptote where the normalized frequency shifts to a higher value (Region B). Now we can estimate the damping coefficient by comparing the transient maximum displacement of the cantilever $u^*(1,t^*)$ between numerical and experimental data for a given value of dimensionless μ_1 and/or μ_2, along with similar dimensionless tip-mass π_4, and dimensionless E-M terms π_3 and π_5.

Piezoelectric cantilevers (TE Connectivity) with dimension of 41 × 17 × 0.2 mm^3 (i.e. $w = 17$ mm, $t = 0.2$ mm), resistance $R_f = 1{\times}10^{-7}$ Ohms, capacitance $C_f = 1.38{\times}10^{-9}$ F and $\alpha = 1.7{\times}10^{-8}$ N/V (Newtons per Volt) were used for experiments. The other properties, for the composite structure, we estimated as $E = 3{\times}10^{-9}$ (an average value) and $\rho = 1800$ kg/m^3. The experimental setup consisted of two acrylic bridges made of 60 mm high and 12 mm thick vertical posts supported by a 19.0 mm thick base, erected inside an open circuit wind tunnel. The distance between the two bridges was 115 mm. Two piezoelectric strips were mounted individually on an acrylic cube (13 × 13 × 13 mm^3), and the cube was bolted to the vertical posts. Thus, the piezoelectric cantilevers possess 1-DOF and vibrate along their transverse direction. The approximate cantilever length measured from acrylic cube to mass-free tip that was free to vibrate was $L = 25$ mm, although this length may need to be adjusted when computing natural frequency since the attached tip-mass can reduce this value. With this length the corresponding electrical dimensionless parameter are $\pi_3 \approx 0.31$ with $\omega \approx 120$ Hz and $\pi_5 \approx 1.5 \times 10^{-4}$. A decrease in the vibration length L results in an increased ω and smaller π_3 and slightly larger π_5.

We used tip masses in the form of rectangular prisms made of dense tear-resistant foam sheet (McMaster-Carr) loaded onto the piezoelectric films. Two thicknesses, 12.7 mm and 19.0 mm, were used for the models. To attach the prisms onto the PZT cantilevers, slits 16 mm wide with negligible thickness were laser cut (Epilog) on the test pieces. However, for a select few, a razor blade was used to make slits on the rectangle's short face because the short face was prone to laser burns. A total of 11 test pieces with B-by-D (B/D) ratios ranging from 0.5 to 3.0 were made and were loaded onto the piezoelectric cantilevers, resulting in dimensionless mass ratios $2 < \pi_4 < 5$. In a separate set of experiments, an oscilloscope (Model DSO1024A, Keysight Technologies) was used to record the piezo films' voltage-time data. The oscilloscope possesses a maximum bandwidth of 200 MHz and a sampling size of 2 GSa/s.

The natural frequency was found experimentally for all the B/D ratios by exciting the tip-mass cantilever systems with small displacements. Vibrations of the cantilever tip were captured by a fast camera (Hotshot) at roughly 2000 frames per second, fit with a macro lens (Computar), and in a 500 × 500 pixels window (pixel window and frames per second were subject to change for specific experiments as needed). A fluorescent lamp in line with the camera was placed behind the setup. The experiments were carried out in air at standard am-

bient temperature and pressure. An in-house MATLAB code extracted frame by frame displacement versus time data. Figure 4 shows a plot comparing the experimental

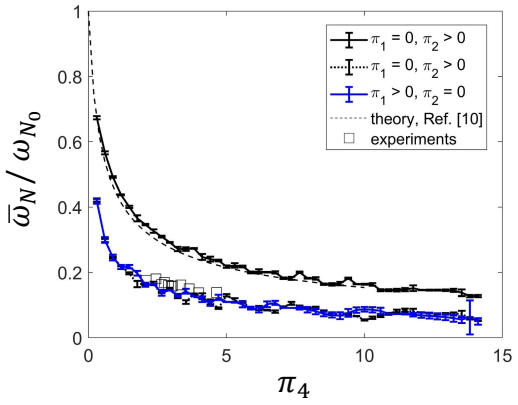

FIG. 5: Plot of normalized averaged natural frequency $\bar{\omega}_N/\omega_{N_0}$ versus dimensionless tip-mass π_4. Data is shown for $\pi_1 = 0$ and $\pi_2 > 0$ averaged at high and low values; $\pi_1 > 0$ with $\pi_2 = 0$; theoretical results for no damping and no rotatory motion of the tip-mass [10]; and measured values from experiments.

and numerical free-end underdamped vibrations of the flexible PZT cantilever tip-mass system versus elapsed time. Similar plots were utilized to estimate the appropriate damping coefficient of a particular system. First, the length L was slightly adjusted until the computed and experimentally measured natural frequency values matched, which resulted in peaks and troughs that were in near-perfect alignment. This required adjustment is not surprising for data where $B/D > 1$ since the reduced length from attaching the tip-mass should affect the natural frequency (See Supplemental Material for more information). A plot of the computed normalized averaged natural frequency $\bar{\omega}_N/\omega_{N_0}$ versus dimensionless tip-mass π_4 appears in Fig. 5. Data is shown for $\pi_1 = 0$ and $\pi_2 > 0$ averaged at high and low values (See Fig. 3), $\pi_1 > 0$ with $\pi_2 = 0$, theoretical results for no damping and no rotatory tip-mass [10], and measured values from experiments. The experiments all fall along the line corresponding to results for viscous and low frequency Kelvin-Voigt damping.

A comparison between maximum voltage $\max|\phi|$ versus initial cantilever displacement appears in Fig. 6. Data is shown comparing values for maximum voltage measured with the oscilloscope and computed. The vertical line corresponds to approximate maximum displacement where computation with Euler-Bernoulli equation is not valid. Although the data is not exact the trends appear similar between the two data sets. This seems to confirm that there is good agreement between the computation and experiments for the range of parameters where the experiments should overlap with the computation. Overall, the results provide a means to estimate damping coefficients that are present in these type of systems.

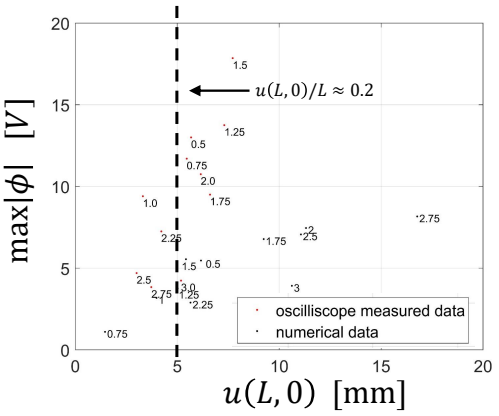

FIG. 6: Plot of maximum voltage $\max|\phi|$ versus initial cantilever displacement. Data is shown for both measured values (oscilloscope) and computed (solutions to governing equations). Note: initial conditions used for computation were randomly selected. Vertical line corresponds to approximate maximum displacement where computation with Euler-Bernoulli equation is not valid.

[1] A. Erturk, D. J. Inman, J. Vibr. Acoust. 130 041002 (2008).
[2] D. Zhu, M. J. Tudor, S. P. Beeby, Meas. Sci. Technol. 21 022001 (2010).
[3] I. Mehdipour, A. Barari, G. Domairry, Computational Materials Science 50, 1830–1833 (2011).
[4] L. Zhao, L. Tang, Y. Yang, Smart Mater. Struct. 22, 125003 (2003).
[5] H. Wang, Q. Meng, Mechanical Systems and Signal Processing 36, 193–209 (2013).
[6] R. L. Harne, C. Zhang, B. Li, K. W. Wang, J. Sound Vib. 373, 206–222 (2016).
[7] M. Zhang, J. Wang, Journal of Sensors 2016, 2673292 (2016).
[8] H. D. Akaydin, N. Elvin, Y. Andreopoulos, Smart Mater. Struct. 21(2), 025007 (2012).
[9] H. T. Banks, D. J. Inman, Trans. ASME 58, 716–723 (1991).
[10] P. A. A. Laura, J. L. Pombo, E. A. Susemihl, J. Sound Vib. 37(2), 161–168 (1974).
[11] S. Lenci, F. Clementi, J. Sound Vib. 331 5247–5267 (2012)
[12] S. Madanu, T. Ward, Chaos 26(6) 063113 (2016).
[13] J. H. Ferziger, *Numerical Methods for Engineering Application*, 2nd ed. (Wiley, New York, 1998).
[14] V. Sajjanapu, T. Ward, J. Fluid Struct. 102, 100290 (2021).